Laser stimulated THz emission from Pt/CoO/FeCoB

Yuta Sasaki[1,2], Guanqiao Li[3], Takahiro Moriyama[4,5]*, Teruo Ono[4,5],
Rostislav V. Mikhaylovskiy[6], Alexey V. Kimel[3], and Shigemi Mizukami[2,7,8]

[1] *Department of Applied Physics, Graduate School of Engineering, Tohoku University, 6-6-05, Aoba-yama, Sendai, Miyagi 980-8579, Japan*
[2] *WPI Advanced Institute for Materials Research (AIMR), Tohoku University, 2-1-1, Katahira, Sendai 980-8577, Japan*
[3] *Radboud University, Institute for Molecules and Materials, Heyendaalseweg 135, Nijmegen, The Netherlands.*
[4] *Institute for Chemical Research, Kyoto University, Gokasho, Uji, Kyoto 611-0011, Japan.*
[5] *Center for Spintronics Research Network (CSRN), Osaka University, Toyonaka, Osaka 560-8531, Japan*
[6] *Department of Physics, Lancaster University, Bailrigg, Lancaster LA1 4YB, United Kingdom*
[7] *Center for Spintronics Research Network (CSRN), Tohoku University, Sendai, Miyagi 980-8577, Japan*
[8] *Center for Science and Innovation in Spintronics (CSIS), Core Research Cluster (CRC), Tohoku University, Sendai 980-8577, Japan*

Abstract

The antiferromagnetic order can mediate a transmission of the spin angular momentum flow, or the spin current, in the form of propagating magnons. In this work, we perform laser stimulated THz emission measurements on Pt/CoO/FeCoB multilayers to investigate the spin current transmission through CoO, an antiferromagnetic insulator, on a picosecond time scale. The results reveal a spin current transmission through CoO with the diffusion length of 3.0 nm. In addition, rotation of the polarization of the emitted THz radiation was observed, suggesting an interaction between the propagating THz magnons and the Néel vector in CoO. Our results not only demonstrate the picosecond magnon spin current transmission, but also the picosecond interaction of the THz magnons with the Néel vector in the antiferromagnet.

*mtaka@scl.kyoto-u.ac.jp

Antiferromagnetic spintronics, where antiferromagnetic materials take on the role of the central active components, is one of the most interesting emerging topics in the field of spintronics today [1,2]. With applications such as THz devices and antiferromagnetic memory devices, many vigorous investigations have been carried out on antiferromagnets including THz spin dynamics [3,4,5,6,7], magnetoresistance [8,9,10,11,12], spin torque effect [13,14], and spin current transmission [15,16,17,18,19,20,21,22].

Among them, spin current transmission in antiferromagnets is quite intriguing. The antiferromagnetic order can mediate the transmission of the spin current in the form of propagating magnons. Several groups have reported this phenomenon in varieties of antiferromagnetic materials, such as NiO [15,16,22], CoO [19], Fe_2O_3 [21], FeMn [20], and IrMn [17]. Most of the investigations have so far been conducted at frequencies much lower than the resonant frequency of the antiferromagnetic materials. In order to explore the physics of the phenomenon, it is crucial to extend the investigation to the THz range , at which antiferromagnets typically have a good susceptibility to electromagnetic field, because this frequency domain embraces the antiferromagnetic resonant frequencies.

A suitable method for investigating antiferromagnetic dynamics is a relatively recently developed technique, where THz radiation is generated with an ultrashort laser pulse in a heavy metal (HM) / ferromagnetic metal (FM) bilayer structure [23,24,25,26]. A femtosecond laser pulse excites an instantaneous non-equilibrium spin current in the FM layer on a sub-picosecond time scale [27,28]. The spin current then flows into the adjacent HM layer. This instantaneous spin current creates an instantaneous charge current by the inverse spin Hall effect in the HM layer, resulting in emission of an electromagnetic wave with the electric field defined by the charge current in the HM layer.

Several groups have investigated the laser stimulated THz emission by inserting a non-magnetic layer (NM) between the FM and the HM, namely HM/NM/FM multilayers [25,29]. It has been found that the efficiency of the THz emission depends on the spin dissipation properties in NM and it decays exponentially with increasing the thickness of the non-magnetic layer. The investigation suggests that the NM layer simply impedes the spin current of sub-picosecond duration with a length scale of the spin diffusion. The same scheme can be applied to explore the transmission of sub-picosecond pulsed spin current in antiferromagnets (AFMs) by investigating HM/AFM/FM multilayers.

In this work, we investigated laser stimulated THz emission from Pt/CoO/FeCoB and explored the sub-picosecond pulsed spin current transmission through the CoO interlayer. We also particularly look into the polarization of the THz electromagnetic wave and reveal that the latter is influenced by the Néel vector in the antiferromagnets.

Multilayers of Pt 5nm/ CoO d_{CoO} nm/$Fe_{40}Co_{40}B_{20}$ 2 nm/SiO_2 5 nm (d_{CoO} = 0 ~ 10 nm) were grown by magnetron sputtering on a single crystal MgO(001) substrate. The Pt and CoO layers were deposited at temperature of 673 K. CoO is a collinear antiferromagnet with a rock-salt crystal structure. It has approximately cubic magnetic anisotropy with the axes along the [100] directions [30] and its Néel temperature is 291 K. Reflective high-energy electron diffraction (RHEED) images after the deposition of the layers Pt and the subsequent CoO layers (see Figs. 1 (a-c)) indicate that the Pt and CoO on MgO(001) were epitaxially grown. The crystallographic orientation of the substrate and the layers in the fabricated structure is MgO(001)[100]//Pt(001)[100]//CoO(001)[100]. The epitaxy maintains up to

d_{CoO} = 10nm (Fig. 1(c)). The films have undergone a field cooling process with an annealing temperature of 473 K and a field of 200 mT applied along the <100> direction. The exchange bias field H_{eb} and coercive field H_c for d_{CoO} = 2 and 5 nm were characterized by magnetization measurements in elevating temperatures as shown in Figs. 1(d,e). The blocking temperature T_B, *i.e.* the temperature at which the exchange bias vanishes, is found to be T_B = 220 K and 280 K for d_{CoO} = 2 and 5 nm, respectively. H_c has a similar trend to H_{eb}. As T_B is generally lower than the Néel temperature, we can assume that these CoO layers maintain the antiferromagnetic order up to T_B. As a reference a sample with SiO_2 interlayer, Pt 5nm/ SiO_2 2 nm/$Fe_{40}Co_{40}B_{20}$ 2 nm/SiO_2 5 nm, was also made by a similar process. All the measurements presented here were performed with blanket films of those multilayers.

Figure 2 shows schematic illustrations of our experimental setup for the laser stimulated THz emission and the polarization measurement. If the spin current raised in FeCoB flows through the CoO layer, the HM layer emits the THz electromagnetic wave (Fig. 2 (a)). We analyzed the electric field component of the emitted THz electromagnetic wave by the electro-optic (EO) sampling technique with 1-mm-thick ZnTe (110)-faced single crystal [31] and two wire grid polarizers [32]. Figure 2 (b) illustrates the geometry of the measurement. The laser incidence is perpendicular to the sample plane. We define the *x*-*y* plane parallel to the sample plane and, therefore, perpendicular to the laser incidence plane. The sample is placed so that the CoO <110> is parallel to the positive *x* axis. The external magnetic field was applied in the positive *x* direction denoted as +*H* while the field components of the THz wave parallel to the *x* and *y* axis, denoted as E_x and E_y respectively, are recorded. We then define the rotation of the polarization of the electric field as $\varphi = \tan^{-1}(|E_x|/|E_y|)$, as indicated in Fig. 2(b).

The polarization of the emitted THz wave is parallel to the electric field induced $\boldsymbol{E}_{\mathrm{c}}$ in the Pt layer. It therefore essentially tells us the polarization direction of the spin current injected into the HM layer through the AFM layer. According to the inverse spin Hall effect, the spin current in the Pt-layer results in the electric field $\boldsymbol{E}_{\mathrm{c}}$ [33] (see Fig. 2 (a)),

$$\boldsymbol{E}_{\mathrm{c}} = Z\left(\theta_{\mathrm{sh}} \int_0^{d_{\mathrm{tot}}} dz\, \boldsymbol{j}_{\mathrm{s}} \times \boldsymbol{\sigma}\right) \quad (1)$$

where Z, θ_{sh}, and d_{tot} are the electro-magnetic impedance of the sample, the spin Hall angle of Pt, and the total thickness of the metallic layer, respectively. $\boldsymbol{\sigma}$ is the spin polarization vector and $\boldsymbol{j}_{\mathrm{s}}$ is the spin current density in the Pt-layer.

Figures 3(a-c) show the wave forms of E_y at room temperature for d_{CoO} = 0, 2, and 5 nm with external magnetic field of $H = +\,100$ mT. E_x is found to be negligibly small. We set $\Delta t = 0$ where E_y peaks. While the shape of the waveform is quite similar regardless of d_{CoO}, the peak field at $\Delta t = 0$, E_y^{peak}, remarkably depends on d_{CoO}. It should be noted that the small oscillations in the range $\Delta t > 1$ ps are found to be due to absorption lines in the spectrum of the remnant moisture (resonant frequencies at around 0.557, 1.168 and 1.80 THz [34]) affecting the experiment. Assuming that 100 mT magnetic field is enough to saturate the magnetization of the FeCoB-layer in the field direction, this result indicates that the direction of the spin density reaching the Pt layer is parallel to the FeCoB magnetization. It implies that the spin current from the FeCoB-layer is transferred to the Pt layer through the CoO interlayer. By performing a similar experiment on the reference sample, we confirmed that the THz wave signal is suppressed when CoO is replaced by SiO_2, which is a non-magnetic insulator (see the dotted line in Fig. 3 (d)). From E_y^{peak} as a function of d_{CoO} shown in Fig. 3(d) the spin-diffusion length λ defined by $A_0 e^{-d_{\mathrm{CoO}}/\lambda}$ is estimated to be 3.0 nm, where A_0 is a constant. This non-zero spin diffusion length are in a good agreement with previous reports of the spin current transmission in antiferromagnets investigated by other measurement techniques [16,17,18,19,22]. Since magnetic coupling between the CoO and FeCoB layers could be the key for spin current transmission through CoO [18], we further explore the THz emission at lower temperatures where the exchange bias emerges.

Figures 4 (a, b) show the wave forms of E_x and E_y for d_{CoO} = 2.0 nm in the magnetic field of two polarities with the strength of 100 mT. In this series of measurements, we first cooled down the sample to 80 K with the magnetic field of 100 mT applied in the same direction as that during the measurements shown in Figs. 2 and 3. The additional measurements were then performed at elevating temperatures while the magnetic field remains on. By using this field application sequence, we make sure to saturate the magnetization in the field direction. The sample thus retains the exchange bias until the blocking temperature T_B. Although E_x is always much smaller than E_y, the former clearly emerges and becomes more pronounced at lower temperature. The wave forms of both E_x and E_y are inverted by flipping the magnetic field direction, indicating that the spin density direction $\boldsymbol{\sigma}$ of the spin current injected into the Pt layer correlates with the orientation of the magnetization of the FeCoB-layer. While E_y can be explained by the spin current transmission with $\boldsymbol{\sigma}$ parallel to the FeCoB magnetization (see Eq. (1)), emergence of E_x suggests that $\boldsymbol{\sigma}$ indeed acquires an orthogonal component to the FeCoB magnetization. Figures 4(c, d) summarize E_y^{peak}, and φ as a function of temperature for d_{CoO} = 0, 2.0, and 5.0 nm. Due to a slight misalignment of the optics, signal fluctuation and other factors, we found there is always a small residual peak in the E_{x} wave form as one can see the data above 200 K for d_{CoO} = 2.0 shown in Fig. 4(b). The samples with d_{CoO} = 0 also show the similar residual peak in the E_{x} wave form. These residual peaks result in the offset of φ below which the value is insignificant as indicated by the hatched area in Fig. 4 (d). We also complementally performed a laser-helicity dependent measurement of the THz emission to rule out the E_x component possibly induced by the inverse spin orbit torque (ISOT) [25,35]. We then found that E_x is nearly independent of the helicity, suggesting that the ISOT contribution to our observed E_x is negligible.

As a general trend, E_y^{peak} decreases with decreasing the temperature regardless of d_{CoO}, which is associated with the temperature dependence of the impedance Z of the sample and spin Hall resistivity of the Pt layer [36]. It is noticeable that the variation of φ with respect to temperature is more pronounced with thicker CoO. By referencing the little variation of φ for d_{CoO} = 0, one can notice that φ apparently increases at lower temperature and has an onset at around 200 K and 300 K for d_{CoO} = 2.0 and 5.0 nm, respectively, which coincide with T_B for these samples (see Fig. 2 (d)). These results suggest that the emergence of E_x is associated with the emergence of the exchange bias in the antiferromagnetic CoO.

We now come to the detail discussions of the experimental results. Considering that CoO is a good insulator with a bandgap of ~2.6 eV [37] and comparing with the data of the SiO_2 interlayer, we assume that charge transfer through the CoO interlayer is also insignificant. The estimated spin diffusion length of λ = 3.0 nm can only be explained by the spin angular momentum carried by magnons in the CoO interlayer as explained in Ref. 19. Therefore, it can be seen here that femtosecond laser excitation launches the spin current from FeCoB to CoO. With the help of magnons in CoO the spin current propagates through the interlayer and reaches the interface CoO/Pt. In the Pt-layer the spin current is converted into the electric field due to the inverse spin Hall effect. We should emphasize that sub-picosecond duration of the spin-current pulse implies the spin transfer through antiferromagnetic CoO is mediated by THz magnons with about 100 times higher frequency than that of magnons employed for spin transport in Ref. 19.

Dominant E_y essentially indicates that the spin current transmitted through the CoO maintains its polarity of the spin density $\boldsymbol{\sigma}$ in the same direction as the FeCoB magnetization. Based on the conservation of spin angular momentum in the diffusive system, it is natural that the polarity of the spin density $\boldsymbol{\sigma}$ from the FeCoB-layer is conserved. The most interesting observation is the non-zero E_x below T_B. If the CoO-layer simply exercised a random scattering of the spin angular momentum, a component of $\boldsymbol{\sigma}$ orthogonal to the FeCoB magnetization would not survive and E_y would only be observed. The emergence of E_x below T_B strongly indicates that the spin scattering is slanted by the antiferromagnetic order in the CoO-layer. This could be a consequence of a twisting of the Néel vector induced in the CoO-layer due to the exchange coupling with the FeCoB-layer. Such a twisting has been previously reported for antiferromagnets and explained in terms of the restorative force of the exchange bias [38]. When the magnetic field $\pm H$ is applied in the direction of <±1±10>, the CoO Néel vector initially stays in one of the [100] directions, which is an easy axis of CoO [30], the field cooling process would then generate a twisting to accommodate the rotation of the FeCoB magnetization into the direction of the field (see Fig. 2(b)). The spin current carried by the THz magnon will then experience a non-uniform scattering background which preferentially scatters the spin orthogonal to the Néel vector gradually rotating away from the axis of the FeCoB magnetization [39]. This essentially rotates the polarity of the spin density $\boldsymbol{\sigma}$ away from the FeCoB magnetization as it reaches the Pt-layer. Therefore, according to Eq. 1, $\mathbf{E}_c$ rotates over φ and E_x emerges. E_x disappears as the Néel vector twisting vanishes above T_B associating with the degradation of the exchange bias. The temperature dependence of

φ thus reflects the Néel vector inhomogeneity in the CoO-layer.

This observation is basically consistent with previous reports on the spin pumping experiments in exchange biased systems [20] and the spin-flopped systems [40] where the spin current impedance was modified by the accommodation of Néel vector twisting. The present experiment detects, instead of the dissipated part of the spin current, the surviving part of the spin current which is collinear to the Néel vectors [41].

In summary, we performed laser stimulated THz emission measurements on Pt/CoO/FeCoB mutilayers. Sub-picosecond pulsed spin current induced by the femtosecond laser pulse is found to transmit through the CoO-layer, an antiferromagnetic insulator, with a spin diffusion length scale of 3.0 nm. Our results are consistent with the explanation that spin angular momentum is carried by magnons in the antiferromagnetic CoO [15,16,17,18,19,20,21,22,40,41]. Above T_B, the polarization of the emitted THz electric field essentially reflects the polarization of the spin current stimulated in the FeCoB-layer. On the other hand, below T_B, the polarization of the emitted THz electric field rotates reflecting the Néel order inhomogeneity in CoO. We presume that the Néel vector twisting below T_B, which gives rise to a slanted spin scattering of the transmitted THz magnon, could be responsible for the rotation of the THz polarization. Therefore, our results not only demonstrate the sub-picosecond spin current transmission in the antiferromagnet, but also the sub-picosecond interaction of the spin current with the Néel order.

Acknowledgements

Y.S. acknowledges the Graduate Program in Spintronics (GP-Spin) at Tohoku University. Authors would like to thank Prof. Se Kwon Kim for the fruitful discussion and valuable comments to the manuscript. This work was supported by JSPS KAKENHI Grant Numbers 17H04924, 17H05181, 19K21972, and 26103004, and by CSRN, and was partly promoted by Collaborative Research Program of the Institute for Chemical Research, Kyoto University.

Data availability

The data that support the findings of this study are available from the corresponding author upon reasonable request.

Figure captions:

Fig. 1 RHEED images after the deposition of the CoO for d_{CoO}=(a) 0, (b)2.0, and (c) 10.0 nm, respectively. (d) Exchange bias field H_{eb} and (e) coercive field H_c as a function of temperature. Red and blue solid circle show the data for d_{CoO}=2.0 and 5.0 nm, respectively.

Fig. 2 Schematic image of (a) the laser stimulated spin current flow in the heavy metal (HM) / antiferromagnetic (AFM) insulator / ferromagnetic metal(FM) structure, and (b) the configuration of the experiment. $\boldsymbol{\sigma}$, $\boldsymbol{j}_s$, and $\boldsymbol{E}_c$ are the spin moment, spin current, and electric field vector, respectively. Magnetic field was applied along x direction and the (110) direction. m_{FCB}, $\bar{n}_{\mathrm{CoO}}$, and φ are the magnetic moment in FeCoB, Néel vector in CoO, and the polarization angle of the THz electromagnetic wave, respectively.

Fig. 3 THz wave forms measured at room temperature with an applied magnetic field parallel to <100> orientation for the films with d_{CoO}=(a) 0, (b)2.0, and (c) 5.0 nm., respectively. (d) d_{CoO} dependence of the peak intensity of THz wave signal E_y^{peak}. Solid curve shows fitting result. Dashed line shows the data for the film with SiO_2 layer.

Fig. 4 (a) The y component E_y and (b) x component E_x of THz wave at various temperatures for the d_{CoO}=2.0 nm film. The positive (+H) and negative (-H) magnetic field was applied along x direction which are shown in red and blue, respectively. (c)The peak value of y component E_y^{peak} and (d) polarization angle of THz electromagnetic wave φ as a function of temperature. Open circle, triangle, and square are the data for d_{CoO} = 0, 2.0, and 5.0 nm, respectively. The hatched area in (d) indicates the offset of φ due to the measurement limit, below which the values are insignificant.

1 **References**

[1] V. Baltz, A. Manchon, M. Tsoi, T. Moriyama, T. Ono, and Y. Tserkovnyak, Rev. Mod. Phys. **90**, 015005 (2018).
[2] T. Jungwirth, X. Marti, P. Wadley, and J. Wunderlich, Nat. Nanotechnol. **11**, 231 (2016).
[3] T. Kampfrath, A. Sell, G. Klatt, A. Pashkin, S. Meahrlein, T. Dekorsy, M. Wolf, M. Fiebig, A. Leitenstorfer, and R. Huber, Nat. Photon. **5**, 31 (2011).
[4] T. Moriyama, K. Hayashi, K. Yamada, M. Shima, Y. Ohya, and T. Ono, Phys. Rev. Mater. **3**, 051402 (2019).
[5] T. Satoh, S.-J. Cho, R. Iida, T. Shimura, K. Kuroda, H. Ueda, Y. Ueda, B. A. Ivanov, F. Nori, and M. Fiebig, Phys. Rev Lett. **105**, 077402 (2010).
[6] J. Nishitani, T. Nagashima, and M. Hangyo, Phys. Rev. B **85**, 174439 (2012).
[7] S. Baierl, J. H. Mentink, M. Hohenleutner, L. Braun, T.-M. Do, C. Lange, A. Sell, M. Fiebig, G. Woltersdorf, T. Kampfrath, and R. Huber, Phys. Rev. Lett. **117**, 197201 (2016).
[8] X. Marti, I. Fina, C. Frontera, J. Liu, P. Wadley, Q. He, R. J. Paull, J. D. Clarkson, J. Kudrnovský, I. Turek, J. Kuneš, D. Yi, J. Chu, C. T. Nelson, L. You, E. Arenholz, S. Salahuddin, J. Fontcuberta, T. Jungwirth, and R. Ramesh, Nat. Mater. **13**, 367 (2014).
[9] T. Moriyama, N. Matsuzaki, K.-J. Kim, I. Suzuki, T. Taniyama, and T. Ono, Appl. Phys. Lett. **107**, 122403 (2015).
[10] G. R. Hoogeboom, A. Aqeel, T. Kuschel, T. T. M. Palstra and B. J. van Wees, Appl. Phys. Lett. **111**, 052409 (2017).
[11] M. Kimata, T. Moriyama, K. Oda and T. Ono, Appl. Phys. Lett. **116**, 192402 (2020).
[12] T. Iino, T. Moriyama, H. Iwaki, H. Aono, Y. Shiratsuchi, T. Ono, Appl. Phys. Lett. **114**, 022402 (2019)
[13] P. Wadley, B. Howells, J. Elezny, C. Andrews, V. Hills, R. P. Campion, V. Novak, K. Olejnik, F. Maccherozzi, S. S. Dhesi, S. Y. Martin, T. Wagner, J. Wunderlich, F. Freimuth, Y. Mokrousov, J. Kune, J. S. Chauhan, M. J. Grzybowski, A. W. Rushforth, K. W. Edmonds, B. L. Gallagher, and T. Jungwirth, Science **351**, 587 (2016).
[14] T. Moriyama, K. Oda, T. Ohkochi, M. Kimata, and T. Ono, Sci. Rep. **8**, 14167 (2018).
[15] H. Wang, C. Du, P. C. Hammel, and F. Yang, Phys. Rev. Lett. **113**, 097202 (2014).
[16] T. Moriyama, S. Takei, M. Nagata, Y. Yoshimura, N. Matsuzaki, T. Terashima, Y. Tserkovnyak, and T. Ono, Appl. Phys. Lett. **106**, 162406 (2015).
[17] L. Frangou, S. Oyarzún, S. Auffret, L. Vila, S. Gambarelli, and V. Baltz, Phys. Rev. Lett. **116**, 077203 (2016).
[18] S. Takei, T. Moriyama, T. Ono, Y. Tserkovnyak, Phys. Rev. B **92**, 020409R (2015).
[19] Z. Qiu, J. Li, D. Hou, E. Arenholz, A. T. N'Diaye, A. Tan, K.-i. Uchida, K. Sato, S. Okamoto, Y. Tserkovnyak, Z. Q. Qiu, and E. Saitoh, Nat. Commun. **7**, 12670 (2016).
[20] T. Moriyama, M. Kamiya, K. Oda, K. Tanaka, K.-J. Kim, and T. Ono, Phys. Rev. Lett. **119**, 267204 (2017).
[21] R. Lebrun, A. Ross, S. A. Bender, A. Qaiumzadeh, L. Baldrati, J. Cramer, A. Brataas, R. A. Duine and M. Kläui, Nature **561**, 222 (2018).
[22] Y. Wang, D. Zhu, Y. Yang, K. Lee, R. Mishra, G. Go, S.-H. Oh, D.-H. Kim, K.Cai1 , E. Liu, S. D. Pollard , S. Shi , J. Lee , K. L. Teo, Y. Wu, K.-J. Lee, H. Yang, Science **366**, 1125-1128 (2019).
[23] T. S. Seifert, N. M. Tran, O. Gueckstock, S. M. Rouzegar, L. Nadvornik, S. Jaiswal, G. Jakob, V. V. Temnov, M. Münzenberg, M. Wolf, M. Kläui and T. Kampfrath, J. Phys. D: Appl. Phys. **51**, 364003 (2018).
[24] J. Cramer, T. Seifert, A. Kronenberg, F. Fuhrmann, G. Jakob, M. Jourdan, T. Kampfrath, and M. Klaui, Nano. Lett. **18**, 1064-1069 (2018).
[25] Y. Wu, M. Elyasi, X. Qiu, M. Chen, Y. Liu, L. Ke, and H. Yang, Adv. Mater. **29**, 1603031

(2017).
26 M. Chen, R. Mishra, Y. Wu, K. Lee and H. Yang, Adv. Opt. Matter. **6**, 1800430 (2018).
27 T. Kampfrath, M. Battiato, P. Maldonado, G. Eilers, J. Nötzold, S. Mährlein, V. Zbarsky, F. Freimuth, Y. Mokrousov, S. Blügel, M. Wolf, I. Radu, P. M. Oppeneer, and M. Münzenberg, Nat. Nanotech. **8**, 256-260 (2013).
28 T. S. Seifert, S. Jaiswal, J. Barker, S. T. Weber, I. Razdolski, J. Cramer, O. Gueckstock, S. F. Maehrlein, L. Nadvornik, S. Watanabe, C. Ciccarelli, A. Melnikov, G. Jakob, M. Münzenberg, S. T. B. Goennenwein, G. Woltersdorf, B. Rethfeld, P. W. Brouwer, M. Wolf, M. Kläui and T. Kampfrath, Nat. Commun. **9**, 2899 (2018).
29 G. Li, R. V. Mikhaylovskiy, K. A. Grishunin, J. D. Costa, Th. Rasing, and A. V. Kimel, J. Phys. D: Appl. Phys. **51**, 134001 (2018).
30 E. Mły´nczak, B. Matlak, A. Kozioł-Rachwał, J. Gurgul, N. Spiridis, and J. Korecki, Phys. Rev. B **88**, 085422 (2013).
31 G. Gallot and D. Grischkowsky, J. Opt. Soc. Am. B **16**, 1204 (1999).
32 T. Huisman, R. V. Mikhaylovskiy, Th. Rasing, A. V. Kimel, A. Tsukamoto, B. Ronde, L. Ma, W. J. Fan, and S. M. Zhou, Phys. Rev. B **95**, 094418 (2017).
33 T. Seifert, S. Jaiswal, U. Martens, J. Hannegan, L. Braun, P. Maldonado, F. Freimuth, A. Kronenberg, J. Henrizi, I. Radu, E. Beaurepaire, Y. Mokrousov, P. M. Oppeneer, M. Jourdan, G. Jakob, D. Turchinovich, L. M. Hayden, M. Wolf, M. Münzenberg, M. Kläui and T. Kampfrath, Nature Photon. **10**, 483 (2016).
34 D. M. Mittleman, R. H. Jacobsen, R. Neelamani, R. G. Baraniuk, and M. C. Nuss, Appl. Phys. B **67**, 379-390 (1998).
35 T. J. Huisman, R. V. Mikhaylovskiy, J. D. Costa, F. Freimuth, E. Paz, J. Ventura, P. P. Freitas, S. Blügel, Y. Mokrousov, Th. Rasing and A. V. Kimel, Nature Nanotech. **11**, 455 (2016).
36 M. Matthiesen, D. Afanasiev, J. R. Hortensius, T. C. van Thiel, R. Medapalli, E. E. Fullerton, and A. D. Caviglia, Appl. Phys. Lett. **116**, 212405 (2020).
37 J. van Elp, J. L. Wieland, H. Eskes, P. Kuiper, G. A. Sawatzky, F. M. F. de Groot, and T. S. Turner, Phys. Rev. B **44**, 6090 (1991).
38 D. Mauri, H. C. Siegmann, P. S. Bagus, and E. Kay, J. Appl. Phys. **62**, 3047 (1987).
39 Helen V. Gomonay and Vadim M. Loktev, Phys. Rev. B **81**, 144427(2010).
40 Z. Qiu, D. Hou, J. Barker, K. Yamamoto, O. Gomonay, E. Saitoh, Nat. Mater. **17**, 577 (2018).
41 S. K. Kim, Y. Tserkovnyak, and O. Tchernyshyov, Phys. Rev. B **90**, 104406 (2014).

Figs2_2020revise_TM.pdf

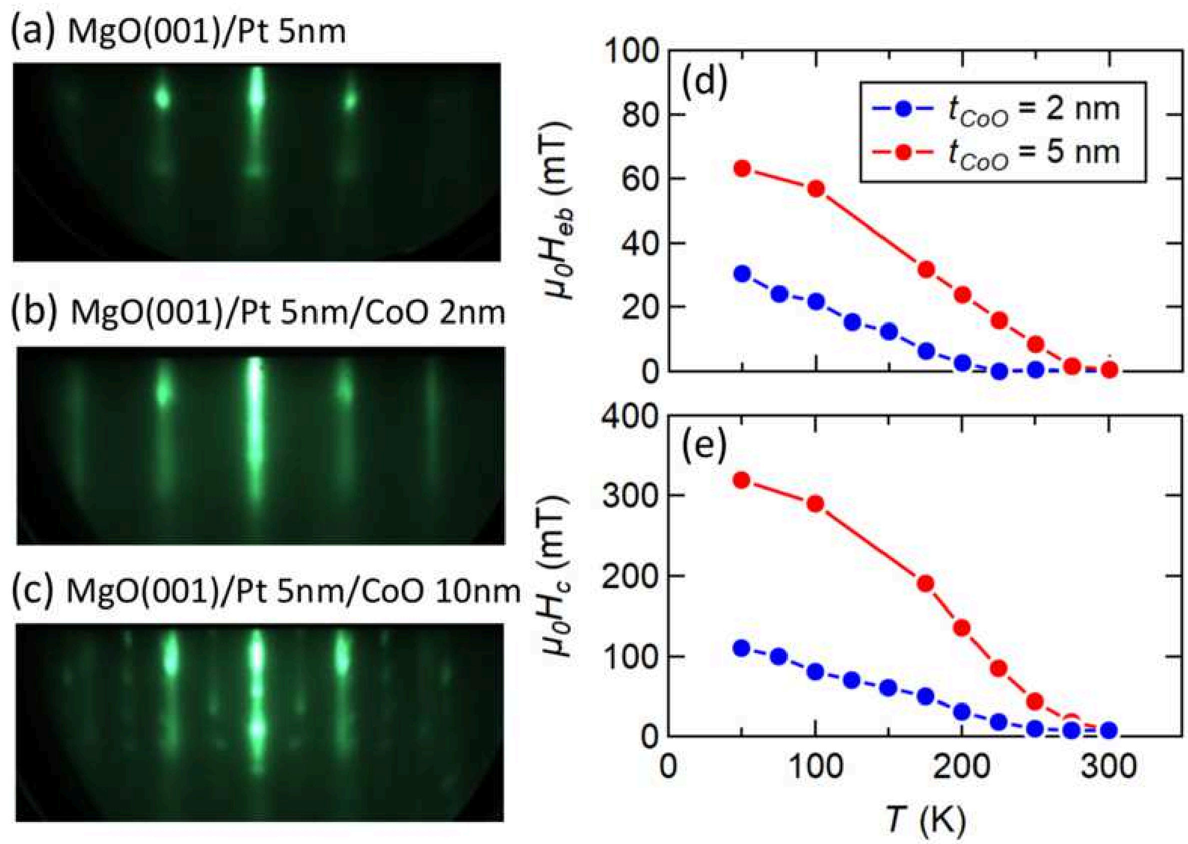

Figs2_2020revise_TM.pdf

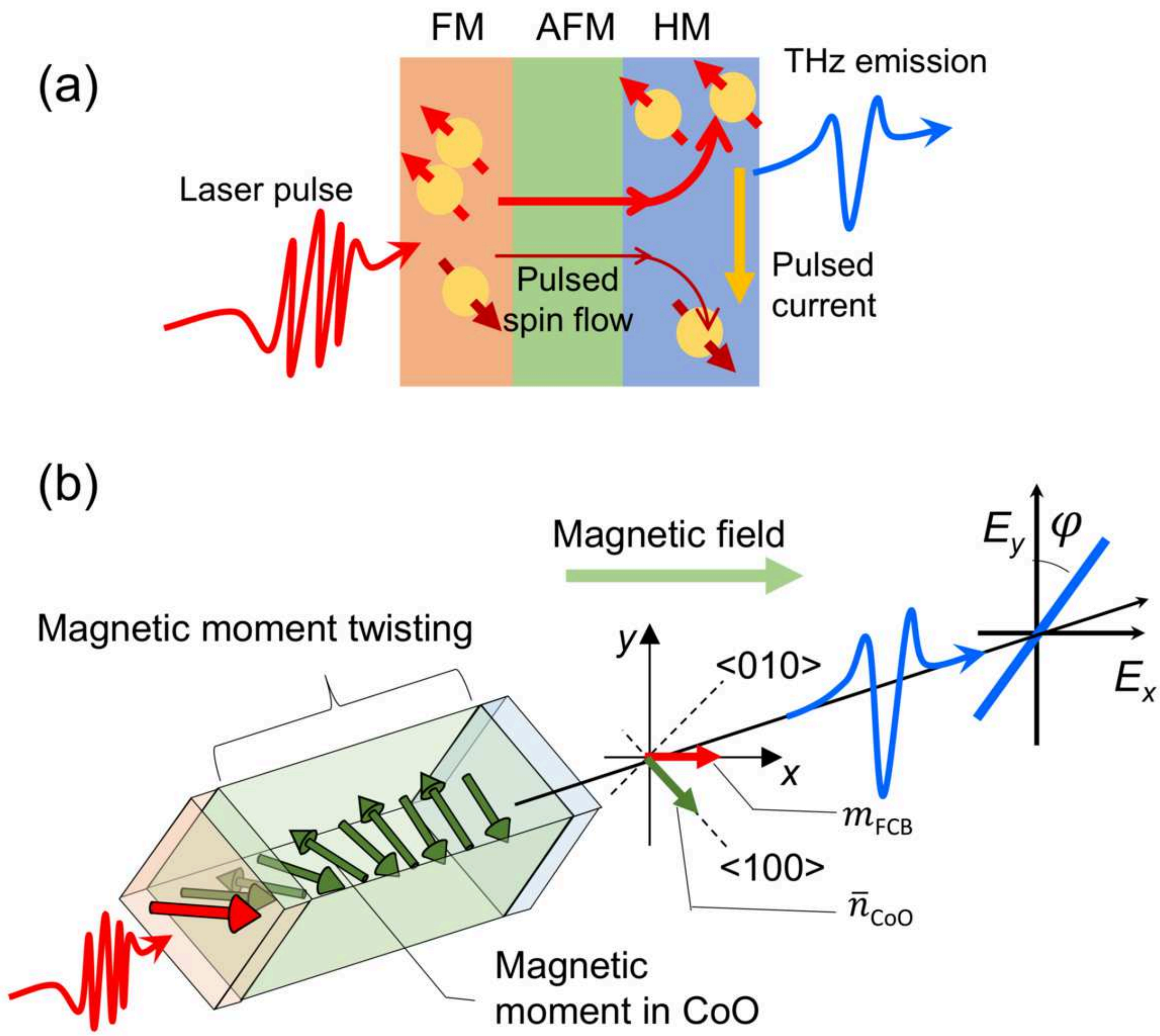

Figs2_2020revise_TM.pdf

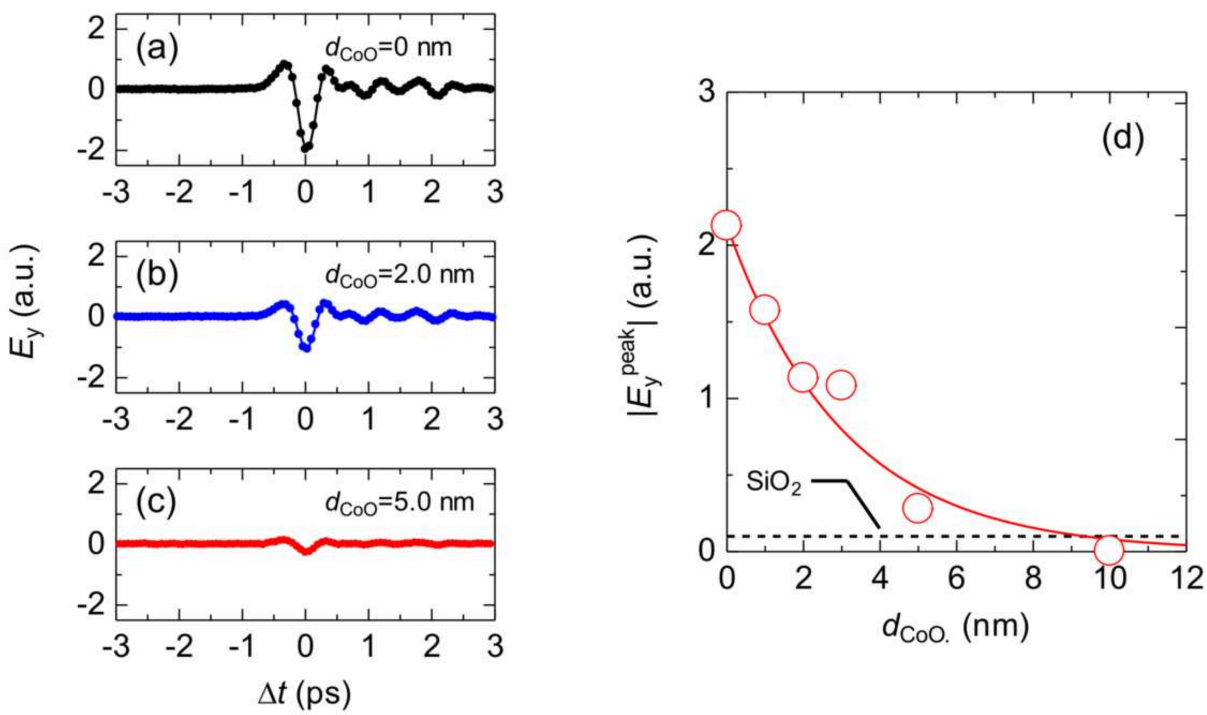

Figs2_2020revise_TM.pdf